METRICA
METRology Institutional CAtalog

ISTITUTO NAZIONALE DI RICERCA METROLOGICA
Repository Istituzionale

Hierarchical Ethyl Cellulose Films With Exceptional UV Stability Enabling Highly Efficient Daytime Radiative Cooling

Original
Hierarchical Ethyl Cellulose Films With Exceptional UV Stability Enabling Highly Efficient Daytime Radiative Cooling / Guo, Xin; Chen, Yanyu; Yan, Dukang; Zhao, Jiupeng; Pan, Lei; Xu, Hongbo; Pattelli, Lorenzo; Li, Yao. - In: SMALL STRUCTURES. - ISSN 2688-4062. - 7:5(2026). [10.1002/sstr.70462]

Availability:
This version is available at: 11696/89699 since: 2026-05-17T18:32:16Z

Publisher:
Wiley-VCH

Published
DOI:10.1002/sstr.70462

Terms of use:

This article is made available under terms and conditions as specified in the corresponding bibliographic description in the repository

Publisher copyright

(Article begins on next page)

29 May 2026

Small Structures

small structures

www.small-structures.com

RESEARCH ARTICLE OPEN ACCESS

Hierarchical Ethyl Cellulose Films With Exceptional UV Stability Enabling Highly Efficient Daytime Radiative Cooling

Xin Guo[1] | Yanyu Chen[2] | Dukang Yan[1] | Jiupeng Zhao[1] | Lei Pan[1] | Hongbo Xu[1] | Lorenzo Pattelli[3,4] | Yao Li[2,5]

[1]School of Chemistry and Chemical Engineering, Harbin Institute of Technology, Harbin, P. R. China | [2]Center for Composite Materials and Structure, Harbin Institute of Technology, Harbin, P. R. China | [3]Istituto Nazionale di Ricerca Metrologica (INRiM), Turin, Italy | [4]European Laboratory for Nonlinear Spectroscopy (LENS), Sesto Fiorentino, Italy | [5]Suzhou Laboratory, Suzhou, China

Correspondence: Lei Pan (panlei@hit.edu.cn) | Hongbo Xu (iamxhb@hit.edu.cn) | Lorenzo Pattelli (l.pattelli@inrim.it) | Yao Li (liyao@hit.edu.cn)

Received: 6 March 2026 | **Revised:** 15 April 2026 | **Accepted:** 1 May 2026

Keywords: eco-friendliness | ethyl cellulose | hierarchical structure | radiative cooling | UV-resistance

ABSTRACT

Flexible radiative cooling materials can dissipate heat from objects without energy consumption, offering a sustainable approach to thermal management. Current research lacks radiative cooling materials combining eco-friendliness and UV resistance. We develop a flexible and eco-friendly ethyl cellulose (EC) film with durable UV resistance via a scalable electrospinning approach, enabling efficient daytime radiative cooling. The EC film has an average solar reflectance of 97.4% (0.3–2.5 μm) and a mid-infrared emittance of 89.4% (8–13 μm), resulting in a theoretical radiative cooling power of 145 W m^{-2}. Therefore, under the solar radiation of 961 W m^{-2}, the EC film achieves a significant temperature reduction of about 10.4°C below the ambient temperature. Since the electron-donation effect of the ethyl group, the ethyl groups can reduce the reactivity of hydroxyl groups and generate sacrificial carbon-centered free radicals to enhance the UV stability of the EC film. After 600 h of continuous UV irradiation at 0.7 kW m^{-2}, the EC film exhibits an average solar reflectivity of 96.9%. Moreover, the EC film degrades naturally in soil within ≈8 months. The excellent refrigeration performance, UV stability, and eco-friendliness of the EC film make it highly promising for diverse refrigeration applications.

1 | Introduction

Passive daytime radiative cooling (PDRC) dissipates excessive heat from the Earth's surface through atmospheric windows (8–13 μm) to the extremely cold outer space (~3 K), thereby passively cooling objects without consuming any energy [1–3]. This can alleviate the problem of traditional refrigeration technology consuming fossil fuels and exacerbating global warming [4–7]. In recent years, this cooling method has attracted more and more attention as an eco-friendly alternative to electric refrigeration. This cooling technology has been applied to various scenarios such as energy-saving buildings, dew collection, personal thermal management, photovoltaic refrigeration, cold storage, and power generation [8].

Early radiation cooling materials are composed of inorganic materials [9–14]. Rephaeli et al. [15] introduced a double-layer photonic crystal with periodically arranged square holes composed of SiC and quartz, and then placed it together with a multilayer structure composed of MgF_2 and TiO_2 on an Ag substrate to synthesize a radiation cooling material, which possesses a net cooling power of more than 100 W m^{-2} at ambient temperature. The rigid nature, complex fabrication process, and high cost of this photonic crystal PDRC material hinder its mass production

This is an open access article under the terms of the Creative Commons Attribution License, which permits use, distribution and reproduction in any medium, provided the original work is properly cited.

© 2026 The Author(s). *Small Structures* published by Wiley-VCH GmbH.

and practical application. In contrast, polymer-based porous PDRC materials are usually simple to prepare and inexpensive, and also have flexibility. With the advancement of research in the field of PDRC, its constituent materials have evolved from inorganic materials to polymers [16–22] and composite materials [23–32]. Correspondingly, the structural design has evolved toward typical configurations, including multilayer and porous structures, to maximize solar reflectivity and mid-infrared (MIR) emissivity. For example, Luo et al. [33] prepared a polyvinylidene fluoride-hexafluoropropylene PDRC material with a multilevel porous structure by the phase inversion method of the solution, which effectively reflects sunlight (solar reflectivity of 96.4%) while also being suitable for mass production and practical application. However, the internal micropore size of the material prepared by the solution phase inversion method is often difficult to control precisely. Song et al. [34] prepared a double-layer radiation cooling fabric using a more mature electrospinning method, which consists of a polyethylene (PE) film with nanopores (100–1000 nm in pore size) and a layer of nylon nanofibers (ca. 100 nm in diameter). This fabric can provide the same wearing comfort as traditional fabrics, while its heat storage capacity is only 1.3 W m^{-2}, demonstrating remarkable heat dissipation capabilities. The polymer-based PDRC material combines radiative cooling capability with mechanical flexibility, thereby providing effective daytime radiative cooling for objects of various shapes and sizes [35].

Nevertheless, many polymers absorb UV radiation and exhibit poor UV-resistance [20, 36, 37]. When exposed to prolonged UV irradiation, these materials undergo photooxidation, leading to chromophore formation and subsequent yellowing, thereby compromising both their cooling performance and long-term durability. Most high-fluorine polymers are resistant to this photooxidation issue [38]. However, the high electronegativity of fluorine atoms in their molecular structure result in poor solubility, thus limiting their processability. To mitigate this problem, researchers have combined polymers with UV-resistant inorganic materials featuring wide bandgaps, such as $BaSO_4$ (~6 eV) [39], Al_2O_3 (~8.8 eV), and SiO_2 (~9 eV) [10], to improve the UV reflectivity of polymer-based radiative cooling materials. For instance, Hsu et al. [40] used a template-free roll-to-roll method to prepare a polydimethylsiloxane (PDMS) film with a double-layer structure consisting of Al_2O_3/PDMS and TiO_2/PDMS. The film has a solar reflectance of 96.0% and a thermal emissivity of 97.0%. The introduction of Al_2O_3 nanoparticles enhances UV reflectivity, which reduces UV absorption by PDMS and TiO_2 and delays the photooxidation of the material. Whereas, the compatibility and interfacial bonding issues between inorganic and organic materials reduce the flexibility of polymer-based PDRC materials while increasing their thickness and density. Moreover, many such materials are neither recyclable nor naturally degradable, exacerbating their environmental burden [41].

Herein, we design a flexible ethyl cellulose (EC) film for highly efficient daytime radiative cooling, which also exhibits UV resistance and eco-friendliness. The EC film containing nanofibers and holes not only performs a high reflectance of 97.4% (0.3–2.5 μm), but also has high emittance of 89.4% (8–13 μm), and its theoretical radiation cooling power reaches 145 W m^{-2}. Hence, under the condition of a solar radiation intensity of 961 W m^{-2}, the EC film achieves a significant cooling effect of about 10.4°C and 5.2°C lower than the ambient and white paper temperature, respectively. The introduction of ethyl groups enhances the UV stability of EC films by inhibiting the formation of unsaturated bonds under UV irradiation. After 600 h of continuous UV irradiation at 0.7 kW m^{-2}, the solar reflectance of the EC film remains at 96.9%, showing negligible change. Due to its excellent weather resistance, the EC film is suitable for fruit and vegetable preservation. In a test on chrysanthemums, it achieves a temperature reduction of ≈13.0°C, which is about 6.3°C lower than that achieved with traditional white paper. This superior radiation cooling capability translates into enhanced preservation performance. Furthermore, after nearly 8 months of natural degradation in soil, the EC film near-completely degrades, effectively reducing environmental pollution. This flexible EC film, with its enhanced radiative cooling performance, not only possesses excellent UV stability but is also eco-friendly, highlighting its potential for advanced refrigeration technologies.

2 | Results and Discussion

2.1 | Design and Fabrication of the Radiative Cooling Film with UV Durability

EC is obtained by ethylating cellulose extracted from lignin (Figure S1d–f). EC possesses a refractive index of ≈1.5 and a negligible extinction coefficient across the UV range, endowing the EC film with UV scattering capabilities and minimizing solar absorption [42–44], while its nonzero extinction coefficient in the atmospheric window of 8–13 μm enhances its infrared emissivity (Figure 1a). Using existing "molecular bonds and wavelengths" databases, molecular bonds and functional groups vibrating in the 8–13 μm range can be identified [45, 46]. EC primarily utilizes C—O—C bonds to provide the desired vibrational absorption within the 8–13 μm atmospheric window (ATR Fourier transform infrared spectroscopy (FTIR-ATR), Figure 1b). This eco-friendly EC film utilizes a hierarchical porous design (Figure S1a–c) and is prepared using a relatively mature electrospinning method (Figure 1c).

Based on Mie scattering theory [47–49], the scattering efficiency of EC films with different fiber diameters and fiber film pore sizes is calculated in the solar wavelength range of 0.25–2.5 μm (Figure 1d,e). The results show that the optimal fiber diameter range is 0.25–0.6 μm and the optimal pore size range is 0.5–2.5 μm. The pore size is defined as the equivalent diameter of the voids within the fiber network. The fiber diameter distribution and pore size distribution of the EC film were analyzed from SEM images using Nano Measure 1.2. We prepared EC films with different spinning solution concentrations (Figure S2a–d) and tested their solar reflectance and MIR emissivity, respectively (Figure S2e, f). As the concentration of the spinning solution gradually increases, the microstructure of the EC film changes from beads to smooth nanofibers, and the nanofiber diameter gradually becomes thicker. Likewise, its average solar reflectance gradually increases (Figure S3a), while the average MIR emissivity remains almost unchanged (Figure S3b). When the spinning solution concentration is 28 wt%, the EC film exhibits the highest reflectivity, and its

26884062, 2026, 5, Downloaded from https://onlinelibrary.wiley.com/doi/10.1002/sstr.70462 by Lorenzo Pattelli - Universita Di Firenze Sistema , Wiley Online Library on [17/05/2026]. See the Terms and Conditions (https://onlinelibrary.wiley.com/terms-and-conditions) on Wiley Online Library for rules of use; OA articles are governed by the applicable Creative Commons License

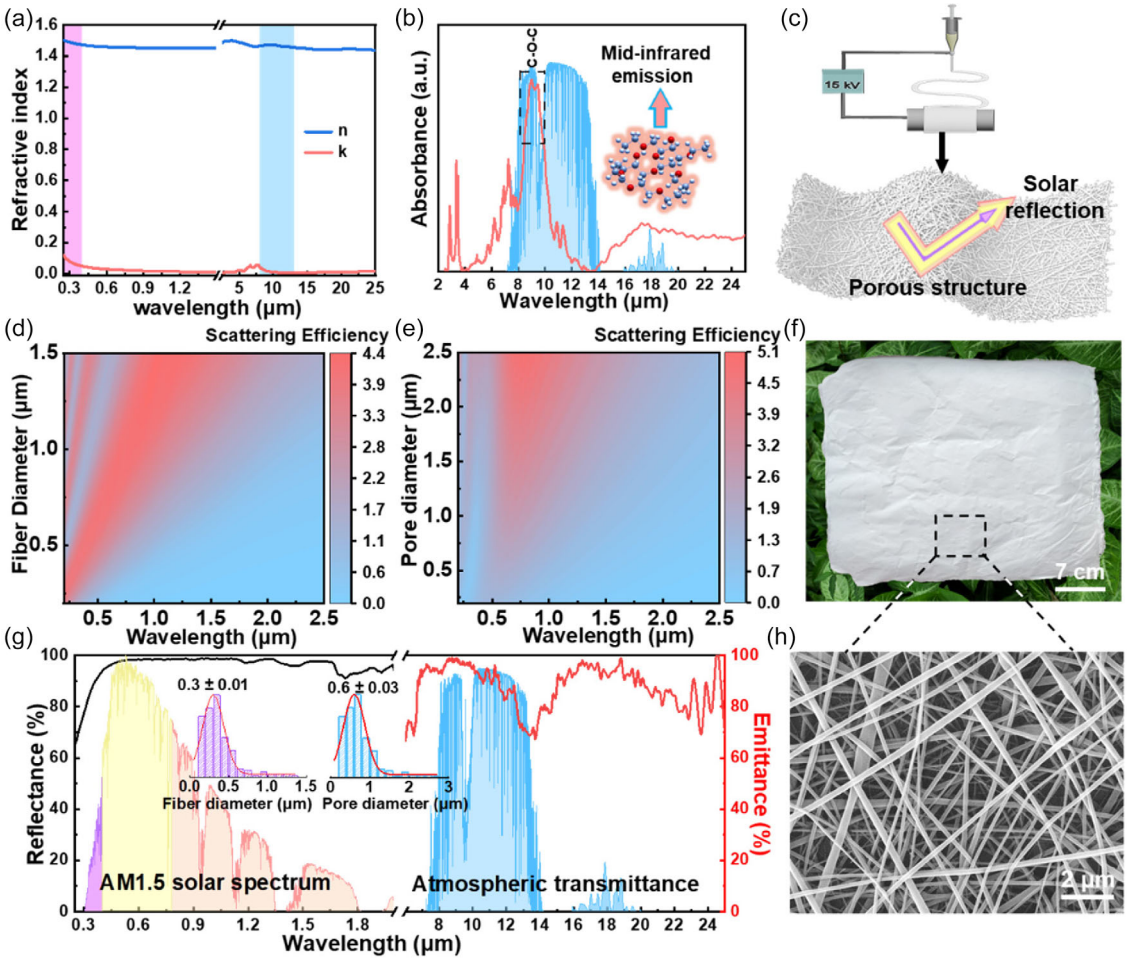

FIGURE 1 | Design and fabrication of the EC film. (a) The complex spectral refractive index ($n + ik$) of EC in the solar and IR wavelength range (0.25–25 μm). (b) FTIR-ATR spectrum of EC films where the main characteristic peaks of C—O—C vibrational absorption/emission of EC are located within the atmospheric window (8–13 μm). (c) Flexible EC films are prepared by electrospinning. Simulated scattering efficiency of EC films as a function of fiber diameter (d) and pore diameter (e) over the wavelength range of 0.25–2.5 μm. (f) Optical image and (h) SEM image of the EC film, revealing a hierarchical porous structure composed of EC nanofibers. (g) Spectral response of the EC film in the 0.25–25 μm waveband, including the solar reflectance (black line) and MIR emittance (red line). The insets show the statistical distribution of the diameters of the EC nanofibers and pores inside the EC film.

fiber diameter and pore diameter are consistent with the simulation results obtained using the finite-difference time-domain method. We tested the solar reflectance and MIR emissivity of EC films with different thicknesses (Figure S4). With increasing film thickness, solar reflectance initially increases and then stabilizes (Figure S5a), while emissivity gradually increases (Figure S5b). When the EC film thickness is ≈340 μm, the material exhibits both high reflectivity and infrared emissivity. The macroscopic and microscopic structures of the optimized EC film are shown in Figure 1f,h, achieving a solar reflectance of 97.4% and an MIR emissivity of 89.4% (Figure 1g). In Mie scattering theory, scattering efficiency is determined by the particle size-to-wavelength ratio. The nanofibers (0.25–0.6 μm) and micropores (0.5–2.5 μm) in our EC films provide complementary spectral coverage across the 0.3–2.5 μm solar spectrum, avoiding the narrow-band scattering peaks typical of single-scale structures. Moreover, the microfiber framework extends the optical path through multiple reflections, while nanopores serve as high-density scattering centers that further scatter light within the interstitial regions. This spatial synergy yields an overall scattering efficiency that exceeds the sum of contributions from individual scales. Notably, the optimized EC film exhibits dual selectivity in the MIR range, as the EC film has a reflectivity and transmittance of over 10% in the 13–16 μm range (Figure S6), which contributes to its excellent performance in radiative cooling.

2.2 | Radiative Cooling Performance of the EC Film

We conducted cooling performance tests using a custom-designed measuring device (Figure 2a). Carbon fiber is used as a substrate to simulate a blackbody due to its strong solar absorptance. The EC film and white paper are separately placed on the carbon fiber, and the substrate temperature was measured under each condition. Figure 2b presents the weather conditions on the test day, where the solar radiation intensity exceeds 600 W m^{-2} and peaks at ≈961 W m^{-2}, along with the real-time temperature profiles. During the high solar radiation period from 12:00 to 13:00, the average ambient temperature is 35.6°C, while the black carbon fiber

26884062, 2026, 5, Downloaded from https://onlinelibrary.wiley.com/doi/10.1002/sstr.70462 by Lorenzo Pattelli - Universita Di Firenze Sistema , Wiley Online Library on [17/05/2026]. See the Terms and Conditions (https://onlinelibrary.wiley.com/terms-and-conditions) on Wiley Online Library for rules of use; OA articles are governed by the applicable Creative Commons License

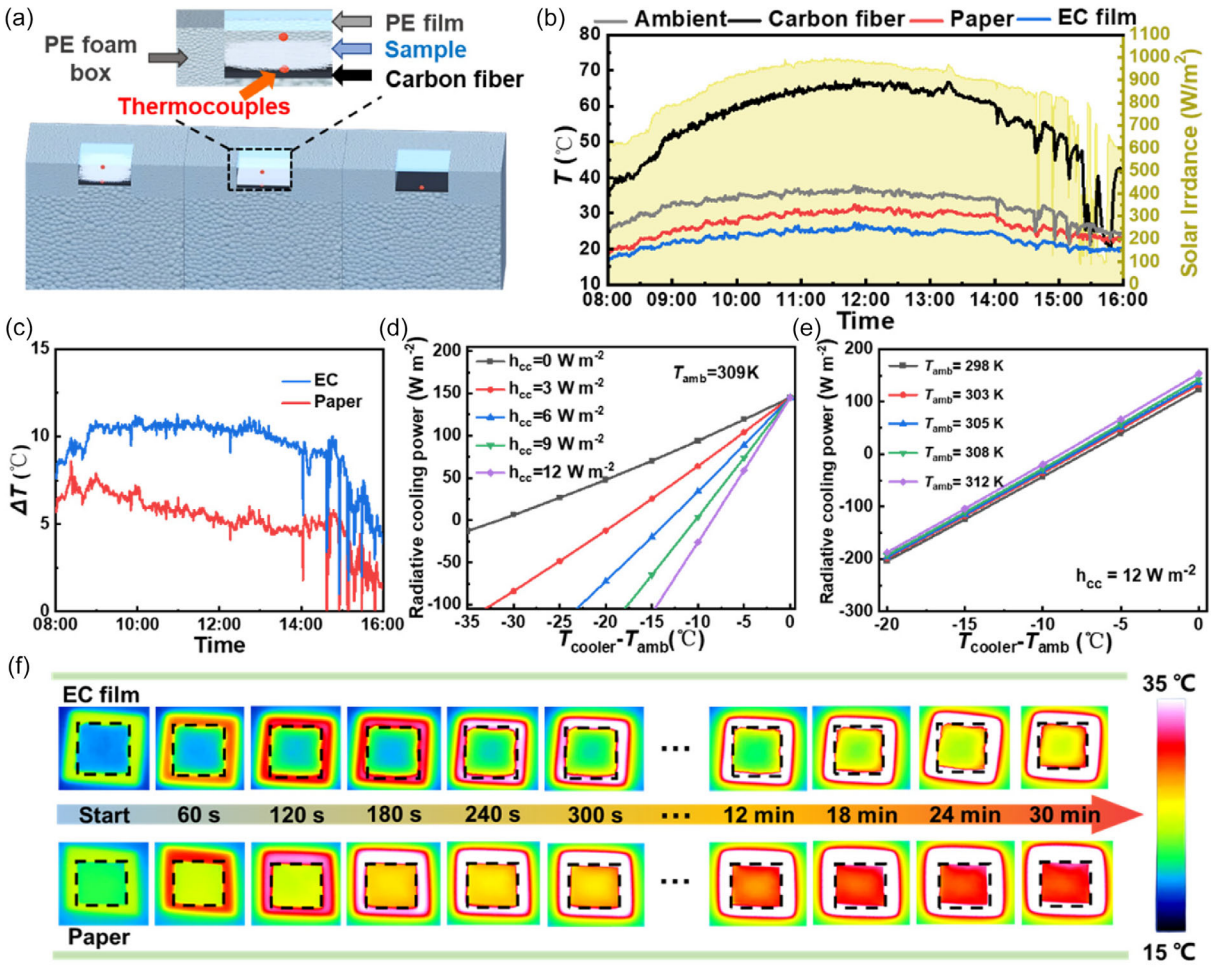

FIGURE 2 | PDRC performance of the EC film. (a) Schematic illustration showing the homemade setup for real-time monitoring of the daytime radiative cooling performance. (b) Temperature (T) and (c) Temperature difference ($\Delta T = T_{amb} - T_{cooler}$) versus time during the outdoor experiment. The yellow area indicates solar intensity versus time during the outdoor experiment at Harbin Institute of Technology, Harbin, China (May 23, 2024, UTC + 8, clear to cloudy sky). (d) Theoretical radiative cooling power of EC films under different h_{cc} (0–12 W m^{-2}) (T_{amb} = 309 K). (e) Theoretical radiative cooling power of EC films at different ambient temperatures (h_{cc} = 12 W m^{-2}). (f) Infrared thermal images of the EC films (4 cm × 4 cm) under different durations of simulated solar irradiation (xenon lamp).

reaches 65.3°C. In contrast, the carbon fiber covered by the EC film remains at ≈25.2°C, corresponding to a temperature drop of about 40.1°C. These results underscore the effective radiative cooling performance of the EC film under real-world conditions. The EC film achieves a cooling of ≈10.4°C below the ambient temperature, notably outperforming white paper, which exhibits a temperature drop of only about 5.2°C under the same conditions (Figure 2c). As mentioned above, the EC film benefits from two key features including strong molecular bond vibration within the atmospheric window and a hierarchical porous structure. These features endow the film with high MIR emissivity and high solar reflectivity, enabling excellent daytime passive radiative cooling performance. The theoretical cooling power of EC film is calculated using the formula in Supplementary Note 2 [14, 50]. Figure 2d shows the cooling power (P_{cool}) of EC film under different nonradiative heat transfer coefficients (h_{cc}). When the temperature of EC film is equal to the ambient temperature (T_{amb} = 309 K), its cooling power is 145 W m^{-2}. With the increase of h_{cc} (0, 3, 6, 9, 12 W m^{-2} K^{-1}), the maximum ΔT obtained is 31.3°C, 18.8°C, 13.4°C, 10.4°C, and 8.5°C, respectively. With the increase of h_{cc}, the maximum ΔT gradually decreases. This demonstrates that the heat conduction and heat convection of the environment will greatly affect the cooling effect of EC film. We also calculated P_{cool} of the EC film at different ambient temperatures (T_{amb}). The results are consistent with the blackbody radiation law, showing that P_{cool} increases with T_{amb} (Figure 2e) [51]. The radiative cooling performance of the film is evaluated using infrared thermal imaging technology (Figure 2f). As the simulated solar radiation time increased, the EC film maintains a low surface temperature of 25°C under half an hour of illumination, while the temperature of the white paper exceeds 30°C. This superior cooling performance is primarily attributed to the EC film's high solar reflectance of 97.4%, significantly exceeding that of white paper (82.5%, Figure S7).

2.3 | Weatherability of the EC Film

To test the potential of EC films for outdoor applications, the weatherability of the EC film is investigated. We first tested hydrophobic and antifouling properties, acid–base corrosion, and thermal stability of EC films. As evidenced by a water contact angle of 140° (Figure S8a), the EC film is hydrophobic. It

26884062, 2026, 5, Downloaded from https://onlinelibrary.wiley.com/doi/10.1002/sstr.70462 by Lorenzo Pattelli - Universita Di Firenze Sistema , Wiley Online Library on [17/05/2026]. See the Terms and Conditions (https://onlinelibrary.wiley.com/terms-and-conditions) on Wiley Online Library for rules of use; OA articles are governed by the applicable Creative Commons License

maintains this high hydrophobicity (contact angles > 120°) even for juice, milk, and inorganic salt solutions (Figure S9), allowing water droplets to be easily removed from its surface [52]. In contrast, the unmodified white paper exhibited hydrophilic behavior (Figure S10), confirming that ethylation modification effectively enhances hydrophobicity. It can be inferred that the microstructure and low surface energy act synergistically to create a surface that resists the adhesion of water molecules. Consequently, dust and contaminants can be readily removed by simply washing with water (Figure S8b, Supplementary Video 1). After cleaning, the EC film retains a high solar reflectance of 96.4%, confirming its excellent antifouling property (Figure S11a). Additionally, its MIR emittance remains almost unchanged (Figure S12a), indicating stable radiative cooling performance. The EC film exhibits excellent chemical stability, retaining an average solar reflectance of 96.1% and 95.8% after 24 h immersion in strong acid and strong base solutions, respectively, compared to its initial 97.4% (Figures S11b,c). This stability is further evidenced by its unchanged MIR emittance (Figure S12b,c). The thermal stability of the EC film is evaluated by thermogravimetric analysis. As shown in Figure S13, the onset decomposition temperature exceeds 200°C, with the maximum decomposition rate occurring at ≈360°C, as determined from the derivative thermogravimetric curve. These results demonstrate the desirable structural stability of EC films at elevated temperatures.

To investigate its resistance to photooxidation, accelerated UV aging tests (0.7 kW m^{-2}, 600 h) are conducted. The results demonstrate the excellent optical stability of the EC film. As shown in Figure 3a, both solar reflectance and MIR emissivity remain stable throughout the test. Specifically, the reflectance stays consistently above 95% (Figure 3b), while the average emissivity exhibits only a gradual increase (Figure S14). In Heilongjiang Province, 600 h of UV irradiation at 0.7 kW m^{-2} corresponds to 400 days of outdoor exposure (based on the calculation in Supplementary Note 3), indicating the EC film's great potential for outdoor applications [53]. In the CIE Lab color space, the b^* value serves as an indicator of yellowing. After 600 h of UV irradiation, the EC film exhibits a Δb^* value of 0, confirming its UV-resistance (Figure S15); its hierarchical porous structure also remains intact (Figure 3c). In contrast, the pristine cellulose exhibits significant photooxidation after 600 h of UV exposure, as evidenced by a Δb^* value increase to 1.64 (indicating pronounced yellowing, Figure S16) and the near-complete disintegration of its fibrous structure (Figure 3d). To elucidate the origin of its superior UV stability, we compared the FTIR-ATR

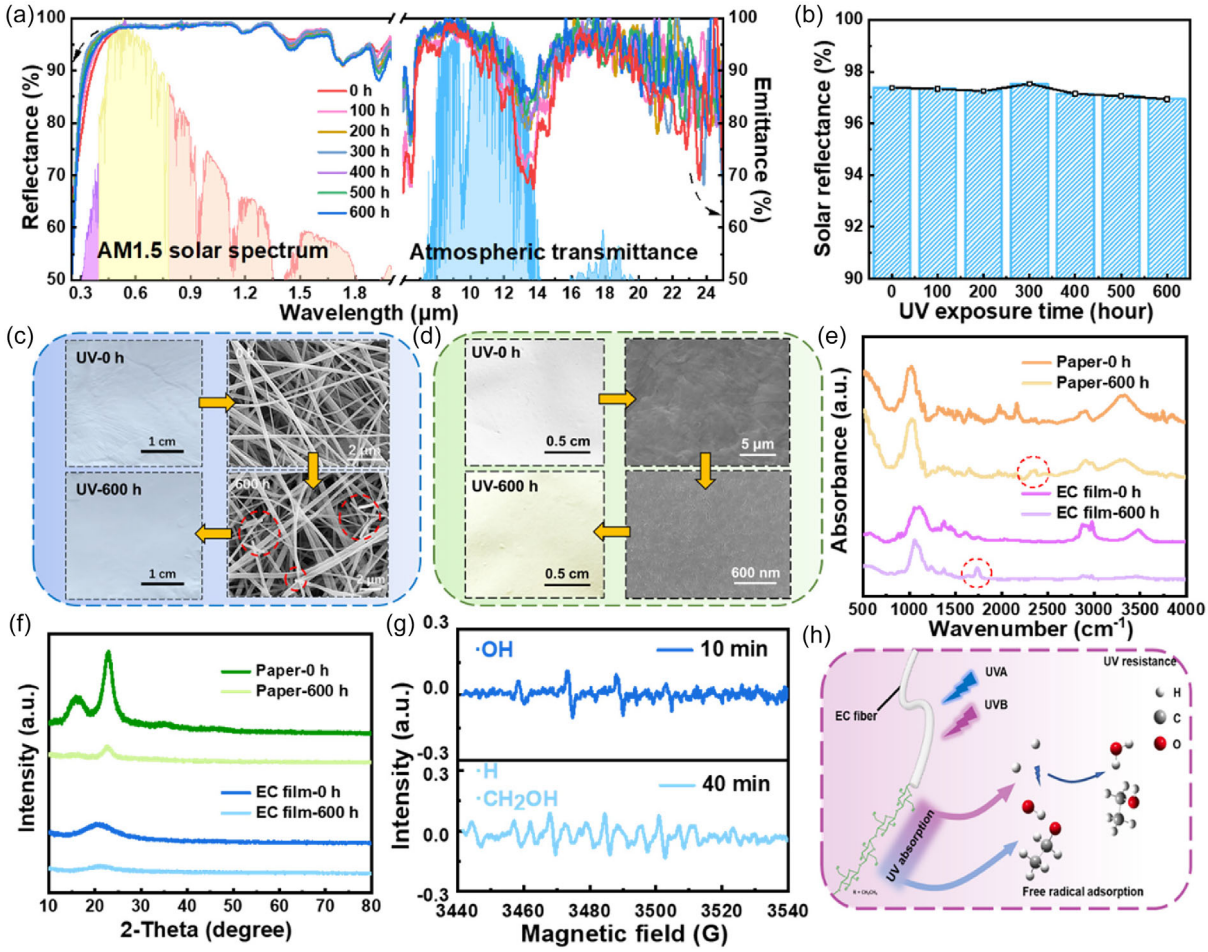

FIGURE 3 | UV durability of the EC film. (a) Solar reflectance and MIR emittance of EC films after 0–600 h of UV irradiation. (b) Average solar reflectance of EC films at different UV irradiation times. (c) EC film and (d) white paper: Optical and SEM images of each, before and after 600 h of UV irradiation. (e) FTIR-ATR spectra and (f) XRD patterns of EC films and paper after different UV irradiation times. (g) EPR spectra of EC films after 10 min and 40 min of simulated solar radiation. (h) Schematic illustration of the UV durability mechanism of EC films.

26884062, 2026, 5, Downloaded from https://onlinelibrary.wiley.com/doi/10.1002/sstr.70462 by Lorenzo Pattelli - Universita Di Firenze Sistema , Wiley Online Library on [17/05/2026]. See the Terms and Conditions (https://onlinelibrary.wiley.com/terms-and-conditions) on Wiley Online Library for rules of use; OA articles are governed by the applicable Creative Commons License

spectra of the EC film and pristine cellulose before and after 600 h of UV exposure (Figure 3e). The EC film shows only minor changes after UV exposure. Specifically, the intensity of hydroxyl and ethyl bands decreases, while only minimal aldehyde groups are formed, confirming its limited photooxidation. Consistent with this, its water contact angle decreases from 140° to 90° (Figure S17), further confirming the partial loss of ethyl groups. This change may affect the long-term durability of the EC membrane in humid or rainy environments, highlighting the need for further optimization of its hydrophobic stability. And the mechanical properties of the EC film deteriorated significantly, with the elastic modulus decreasing from 10.1 to 1.3 MPa (Figure S18), suggesting that further improvement is needed for outdoor applications. Pristine cellulose, by contrast, undergoes severe photooxidation, evidenced by a sharp decrease in hydroxyl groups and the emergence of unsaturated structures (e.g., C≡C, cumulated dienes). X-ray diffraction (XRD) patterns (Figure 3f) reveal decreased crystallinity in both samples, suggesting disruption of hydrogen bonding networks. Nevertheless, the EC film retains a more intact hierarchical porous structure, underscoring its superior structural robustness.

To elucidate the mechanistic role of ethyl groups in EC, we combined DFT calculations with electron paramagnetic resonance (EPR) spectroscopy. The ethoxy group (-OCH_2CH_3), with its strong electron-donating ability, absorbs UV radiation and generates carbon-centered radicals under irradiation (Figure S19; Supplementary Note 4), partially mitigating direct UV radiation impact on the cellulose backbone. The reactions between these generated radicals and hydrogen radicals are thermodynamically spontaneous, with Gibbs free energy changes of 4.81 eV for carbon-centered radicals and 4.01 eV for hydroxyl radicals (Figure S20). This favors the formation of small molecules over backbone attack, thereby reducing chain scission (Figure 3h). EPR spectra provide further evidence for this mechanism (Figure 3g). Under UV irradiation, the EC film exhibits combined signals of hydroxyl radicals ($g \approx 2.0053$), carbon-centered radicals ($g \approx 2.0057$), and hydrogen radicals ($g \approx 2.0054$). In contrast, pristine cellulose shows only hydrogen radical signals ($g \approx 2.0054$, Figure S21), indicating its higher susceptibility to photooxidation compared to the EC film. The EC film exhibits a gradual consumption of ethoxy and hydroxyl groups during 0–300 h of UV exposure, leading to decreased UV radiation absorptance

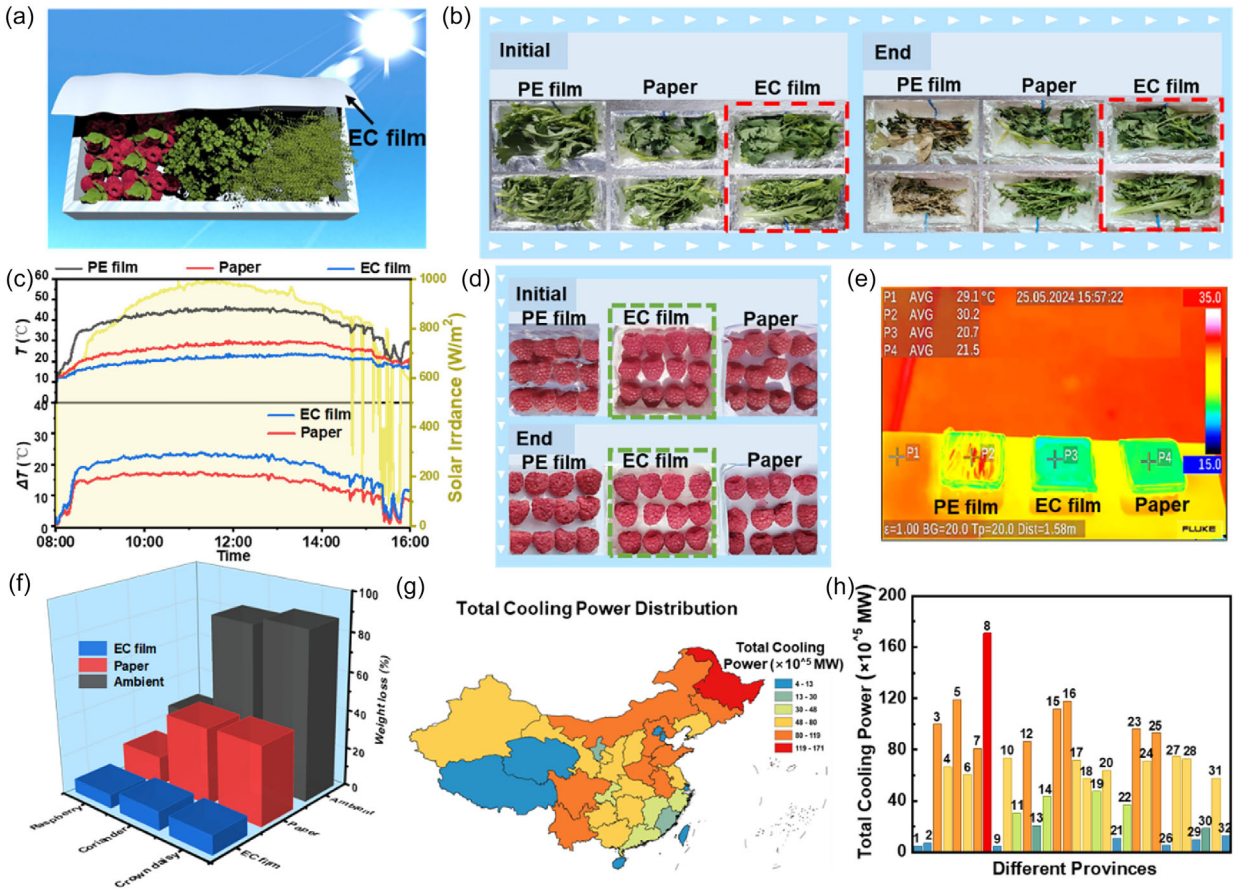

FIGURE 4 | Applicability of the EC film for fresh produce preservation. (a) Schematic of the self-made device for evaluating the cooling performance of EC films on fruits and vegetables. (b) Photographs showing the appearance evolution of vegetables with these packaging films. (c) T and ΔT ($\Delta T = T_{PE} - T_{cooler}$) evolution of crown daisy wrapped with PE films, white paper and EC films during the outdoor experiment located at Harbin Institute of Technology, Harbin, China (May 23, 2024, UTC + 8, clear to cloudy sky). (d) Photographs showing the appearance evolution of raspberries with these packaging films. (e) Infrared image of different covers under direct sunlight in Harbin. (f) Weight loss of crown daisy, coriander and raspberry. (g) The agricultural land statistics for each province in China were obtained from the Institute of Geographic Sciences and Natural Resources Research, Chinese Academy of Sciences (note: number 19 represents Guangdong, Hong Kong, and Macau). (h) Total radiative cooling power in different provinces. Numbers represent different provinces (Table S2, Supporting Information).

26884062, 2026, 5, Downloaded from https://onlinelibrary.wiley.com/doi/10.1002/sstr.70462 by Lorenzo Pattelli - Universita Di Firenze Sistema , Wiley Online Library on [17/05/2026]. See the Terms and Conditions (https://onlinelibrary.wiley.com/terms-and-conditions) on Wiley Online Library for rules of use; OA articles are governed by the applicable Creative Commons License

and increased UV reflectance (Figure S22). Collectively, these results demonstrate that ethyl substitution suppresses photosensitive hydroxyl reactivity, enabling EC films to maintain structural integrity and radiative cooling performance under prolonged UV exposure. Compared with other cellulose-based and flexible radiative cooling materials, the EC film combines high cooling efficiency with long-term outdoor stability, making it an ideal candidate in this field (Supplementary Table S1).

2.4 | The Potential Applicability of the EC Film

The EC film exhibits promising properties for food preservation, including waterproof breathability and mechanical robustness [54, 55]. Its breathability is demonstrated using a simple water-column setup (Figure S23), where under a static pressure of 2.21 kPa, air introduced from one side of the film readily passes through, forming bubbles in the water column on the opposite side (optical image of the EC film after testing in Figure S24). Mechanically, the film shows a tensile elastic modulus of 10.1 MPa (Figure S25; optical image of the EC film in tensile test in Figure S26), indicating favorable load-bearing capacity. The food preservation performance of EC film is evaluated using coriander and crown daisy, two perishable vegetables at room temperature, as model foods. As illustrated in Figure 4a, the vegetables are placed in foam insulation cavities lined with reflective aluminum foil to minimize environmental interference, with the cavities covered by either EC film, PE film, or white paper as the sole heat-exchange interface. After 8 h under natural solar radiation, vegetables packaged with EC film retain their original appearance, while those covered with PE film or white paper show visible shrinkage, rotting, and freshness loss (Figure 4b). Temperature monitoring reveals that chrysanthemums under EC film remain below 23°C at midday—≈13°C below ambient temperature, and 22.5°C and 6.3°C lower than those under PE film and white paper, respectively (Figure 4c). Similar cooling effects are observed for coriander (Figure S27), confirming that EC film effectively cools vegetables under solar exposure. The preservation performance of EC film as a standalone packaging material is further validated using raspberries. After 8 h of solar exposure, raspberries packaged with EC film show minimal deterioration compared to those with PE film or white paper (Figure 4d). Infrared thermal imaging confirms that EC-packaged raspberries maintain the lowest surface temperature throughout the experiment (Figure 4e; Supplementary Video 2), and moisture loss analysis reveals superior water retention with EC film packaging (Figure 4f). With a radiative cooling power of 145 W m^{-2}, the EC film shows promise for food preservation applications. Nationwide deployment as cold-storage film for agricultural products could achieve a total cooling power of 1.9×10^8 MW (Figure 4g,h), offering potential for reducing fossil energy consumption and associated environmental impacts. The radiative cooling capacity of EC films is further confirmed by ice tests: ice blocks wrapped with EC film maintain an average temperature of 2.7°C for 40 min, which is 16.5°C below ambient, while those wrapped with white paper or PE film warm rapidly and melt within 3–11 min (Figure S28).

2.5 | The Environmental Friendliness of the EC Film

To investigate its degradation behavior in a natural environment, EC films and PE nanofilms were placed in soil from April 2, 2024 to November 25, 2024 (Figure 5a). The degradation experiments

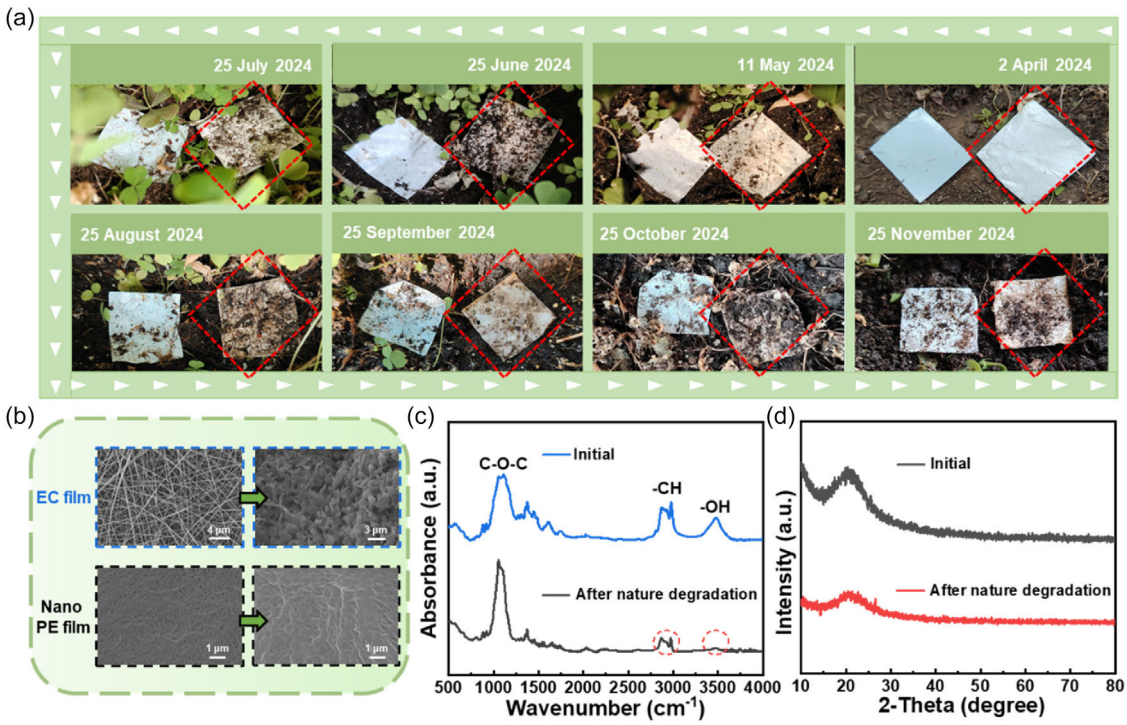

FIGURE 5 | Natural degradation behavior of the EC film. (a) Natural degradation test of the EC film. The EC film is outlined in red for clarity. (b) SEM images of the EC film and the PE nanofilm before and after natural degradation. (c) FTIR-ATR spectra and (d) XRD patterns of EC film before and after natural degradation.

26884062, 2026, 5, Downloaded from https://onlinelibrary.wiley.com/doi/10.1002/sstr.70462 by Lorenzo Pattelli - Universita Di Firenze Sistema , Wiley Online Library on [17/05/2026]. See the Terms and Conditions (https://onlinelibrary.wiley.com/terms-and-conditions) on Wiley Online Library for rules of use; OA articles are governed by the applicable Creative Commons License

were conducted in humus soil with a relative humidity of 60% ± 5% and a temperature of 25 ± 2°C. The samples were buried at a depth of 2–3 cm below the soil surface. After this period, the SEM images of EC films (Figure 5b) reveal that their hierarchical porous structure has gradually disappeared, transforming into fine particles [56], indicating near-complete degradation. In contrast, the PE nanofilm exhibits fiber fusion without breakdown into particles, confirming that this nondegradable PDRC material persists in the environment. Comparison of the FTIR-ATR spectra and XRD patterns before and after degradation (Figure 5c,d) reveals a decrease in hydroxyl and alkyl groups and reduced crystallinity in the degraded EC film, suggesting chain breakage and hydrolysis during natural degradation. The damaged EC film can be dissolved in a homogeneous spinning solution (Figure S29a) and reprocesses into new films via electrospinning. The recycled EC film exhibits an average solar reflectance of 96.4% and maintains high MIR emissivity comparable to the original film (Figures S29b,c), demonstrating the recyclability of this material. This recycling model offers potential for reducing resource waste and environmental impact. Overall, the EC film fabricated via a scalable electrospinning process combines high cooling performance, UV stability, and eco-friendliness, positioning it as a promising candidate for radiative cooling applications.

3 | Conclusion

In summary, we have successfully prepared a UV-resistant radiation cooling EC film using electrospinning technology, with EC as the raw material. Through optical simulation and structural optimization, the EC film achieves a solar reflectance of 97.4% and a MIR emissivity of 89.4%. Under a solar radiation intensity of 961 W m^{-2}, it demonstrates a cooling effect 10.4°C below ambient temperature and 5.2°C below that of white paper. The ethylation modification enhances the optical and chemical stability of cellulose, so that the solar reflectance of EC films remains almost unchanged after 600 h of continuous exposure to 0.7 kW m^{-2} UV irradiation. This offers a strategy for developing UV-resistant polymer-based PDRC materials. Compared with other UV-resistant cooling materials, the EC film not only exhibits its superior UV-resistant performance, but is also eco-friendly and minimizes waste through recyclability. The EC film also exhibits robust weather resistance and favorable mechanical properties, making it suitable for applications such as food preservation and passive refrigeration, with potential for energy savings in a low-carbon society.

Acknowledgments

The authors thank the National Natural Science Foundation of China 52472157 and 5247020620.

Funding

This work was supported by the National Natural Science Foundation of China (52472157 and 5247020620).

Conflicts of Interest

The authors declare no conflicts of interest.

Data Availability Statement

The data that support the findings of this study are available from the corresponding author upon reasonable request.

References

1. X. Yin, R. Yang, G. Tan, and S. Fan, "Terrestrial Radiative Cooling: Using the Cold Universe as a Renewable and Sustainable Energy Source," *Science* 370 (2020): 786, https://doi.org/10.1126/science.abb0971.

2. R. Zevenhoven and M. Falt, "Radiative Cooling through the Atmospheric Window: A Third, less Intrusive Geoengineering Approach," *Energy* 152 (2018): 27, https://doi.org/10.1016/j.energy.2018.03.084.

3. R. W. Bliss Jr., "Atmospheric Radiation near the Surface of the Ground: A Summary for Engineers," *Solar Energy* 5 (1961): 103, https://doi.org/10.1016/0038-092X(61)90053-6.

4. N. Yilmaz and M. Yurtsever, Energy and Climate Change: EurAsia Waste Management Symposium (EWMS), 6, 2022, 782.

5. V. Taseska, N. Markovska, and J. M. Callaway, "Evaluation of Climate Change Impacts on Energy Demand," *Energy* 48 (2012): 88, https://doi.org/10.1016/j.energy.2012.06.053.

6. International Energy Agency (IEA),, The Future of the Refrigeration Industry, 1, 2008, 15, https://www.iea.org/reports/the-future-of-cooling.

7. G. R. Walther, E. Post, P. Convey, et al., "Ecological Responses to Recent Climate Change,"*Nature* 416 (2002): 389, https://doi.org/10.1038/416389a.

8. C. Wang, H. Chen, and F. Wang, "Passive Daytime Radiative Cooling Materials toward Real-World Applications," *Progress in Materials Science* 144 (2024): 101276, https://doi.org/10.1016/j.pmatsci.2024.101276.

9. L. Yang, G. Wang, S. Duan, J. Zhang, and C. Li, "Structurally Colored Photonic Crystal Biomimetic Microstructures for Daytime Radiative Cooling," *ACS Applied Materials & Interfaces* 16 (2024): 62827, https://doi.org/10.1021/acsami.4c10050.

10. X. Zhao, T. Li, H. Xie, et al., "A Solution-Processed Radiative Cooling Glass," *Science* 382 (2023): 684, https://doi.org/10.1126/science.adi2224.

11. K. Lin, S. Chen, Y. Zeng, et al., "Hierarchically Structured Passive Radiative Cooling Ceramic with High Solar Reflectivity," *Science* 382 (2023): 691, https://doi.org/10.1126/science.adi4725.

12. Z. Ding, L. Pattelli, H. Xu, et al., "Iridescent Daytime Radiative Cooling with No Absorption Peaks in the Visible Range," *Small* 18 (2022): 2202400, https://doi.org/10.1002/smll.202202400.

13. H. Bao, C. Yan, B. Wang, X. Fang, C. Y. Zhao, and X. Ruan, "Double-Layer Nanoparticle-Based Coatings for Efficient Terrestrial Radiative Cooling," *Solar Energy Materials and Solar Cells* 168 (2017): 78, https://doi.org/10.1016/j.solmat.2017.04.020.

14. A. P. Raman, M. Abou Anoma, L. Zhu, E. Rephaeli, and S. Fan, "Passive Radiative Cooling below Ambient Air Temperature under Direct Sunlight,"*Nature* 515 (2014): 540, https://doi.org/10.1038/nature13883.

15. E. Rephaeli, A. Raman, and S. Fan, "Ultrabroadband Photonic Structures To Achieve High-Performance Daytime Radiative Cooling," *Nano Letters* 13 (2013): 1457, https://doi.org/10.1021/nl4004283.

16. X. -E. Wu, Y. Wang, X. Liang, et al., "Durable Radiative Cooling Multilayer Silk Textile with Excellent Comprehensive Performance," *Advanced Functional Materials* 34 (2024): 2313539, https://doi.org/10.1002/adfm.202313539.

17. X. Wu, J. Li, F. Xie, et al., "A Dual-Selective Thermal Emitter with Enhanced Subambient Radiative Cooling Performance," *Nature Communications* 15 (2024): 815, https://doi.org/10.1038/s41467-024-45095-4.

18. H. Sun, F. Tang, Y. Bi, et al., "Hierarchically Porous Cellulose Membrane via Self-Assembly Engineering for Ultra High-Power

26884062, 2026, 5, Downloaded from https://onlinelibrary.wiley.com/doi/10.1002/sstr.70462 by Lorenzo Pattelli - Universita Di Firenze Sistema , Wiley Online Library on [17/05/2026]. See the Terms and Conditions (https://onlinelibrary.wiley.com/terms-and-conditions) on Wiley Online Library for rules of use; OA articles are governed by the applicable Creative Commons License

Thermoelectrical Generation in Natural Convection," *Advanced Functional Materials* 33 (2023): 2307960, https://doi.org/10.1002/adfm.202307960.

19. M. Shi, Z. Song, J. Ni, et al., "Dual-Mode Porous Polymeric Films with Coral-Like Hierarchical Structure for All-Day Radiative Cooling and Heating," *ACS Nano* 17 (2023): 2029, https://doi.org/10.1021/acsnano.2c07293.

20. X. Li, Z. Ding, G. E. Lio, et al., "Strain-Adjustable Reflectivity of Polyurethane Nanofiber Membrane for Thermal Management Applications," *Chemical Engineering Journal* 461 (2023): 142095, https://doi.org/10.1016/j.cej.2023.142095.

21. X. Mei, T. Wang, M. Chen, and L. Wu, "A Self-Adaptive Film for Passive Radiative Cooling and Solar Heating Regulation," *Journal of Materials Chemistry A* 10 (2022): 11092, https://doi.org/10.1039/d2ta01291j.

22. T. Li, Y. Zhai, S. He, et al., "A Radiative Cooling Structural Material," *Science* 364 (2019): 760, https://doi.org/10.1126/science.aau9101.

23. Y. Li, X. Zhang, T. Zhang, et al., "Radiative Cooling Materials Prepared by SiO_2 Aerogel microspheres@PVDF-HFP Nanofilm for Building Cooling and Thermal Insulation," *Ceramics International* 50 (2024): 48031, https://doi.org/10.1016/j.ceramint.2024.09.150.

24. Q. Yue, L. Zhang, C. -Y. He, et al., "Polymer Composites with Hierarchical Architecture and Dielectric Particles for Efficient Daytime Subambient Radiative Cooling," *Journal of Materials Chemistry A* 11 (2023): 3126, https://doi.org/10.1039/d2ta07453b.

25. H. Sun, F. Tang, Q. Chen, et al., "A Recyclable, up-Scalable and Eco-Friendly Radiative Cooling Material for All-Day Sub-Ambient Comfort," *Chemical Engineering Journal* 455 (2023): 139786, https://doi.org/10.1016/j.cej.2022.139786.

26. G. Ye, Y. Wan, J. Wu, et al., "Multifunctional Device Integrating Dual-Temperature Regulator for Outdoor Personal Thermal Comfort and Triboelectric Nanogenerator for Self-Powered Human-Machine Interaction," *Nano Energy* 97 (2022): 107148, https://doi.org/10.1016/j.nanoen.2022.107148.

27. D. Miao, N. Cheng, X. Wang, J. Yu, and B. Ding, "Integration of Janus Wettability and Heat Conduction in Hierarchically Designed Textiles for All-Day Personal Radiative Cooling," *Nano Letters* 22 (2022): 680, https://doi.org/10.1021/acs.nanolett.1c03801.

28. D. Han, J. Fei, J. Mandal, et al., "Sub-Ambient Radiative Cooling under Tropical Climate Using Highly Reflective Polymeric Coating," *Solar Energy Materials and Solar Cells* 240 (2022): 111723, https://doi.org/10.1016/j.solmat.2022.111723.

29. S. Zeng, S. Pian, M. Su, et al., "Hierarchical-Morphology Metafabric for Scalable Passive Daytime Radiative Cooling," *Science* 373 (2021): 692, https://doi.org/10.1126/science.abi5484.

30. Z. Cheng, H. Han, F. Wang, et al., "Efficient Radiative Cooling Coating with Biomimetic Human Skin Wrinkle Structure," *Nano Energy* 89 (2021): 106377, https://doi.org/10.1016/j.nanoen.2021.106377.

31. Y. Liu, A. Bai, Z. Fang, Y. Ni, C. Lu, and Z. Xu, "A Pragmatic Bilayer Selective Emitter for Efficient Radiative Cooling under Direct Sunlight," *Materials* 12 (2019): 1208, https://doi.org/10.3390/ma12081208.

32. Y. Zhai, Y. Ma, S. N. David, et al., "Scalable-Manufactured Randomized Glass-Polymer Hybrid Metamaterial for Daytime Radiative Cooling," *Science* 355 (2017): 1062, https://doi.org/10.1126/science.aai7899.

33. M. Luo, J. Liao, X. Wei, et al., "High-Performance Radiative Cooling PVDF-HFP Film Based on Controllable Porous Structure," *Progress in Organic Coatings* 199 (2025): 108901, https://doi.org/10.1016/j.porgcoat.2024.108901.

34. Y. -N. Song, R. -J. Ma, L. Xu, et al., "Wearable Polyethylene/Polyamide Composite Fabric for Passive Human Body Cooling," *ACS Applied Materials & Interfaces* 10 (2018): 41637, https://doi.org/10.1021/acsami.8b14140.

35. J. Li, Y. Liang, W. Li, et al., "Protecting Ice from Melting under Sunlight via Radiative Cooling," *Science Advances* 8 (2022): eabj9756, https://www.science.org/doi/10.1126/sciadv.abj9756.

36. C. Maraveas, I. V. Kyrtopoulos, K. G. Arvanitis, and T. Bartzanas, "The Aging of Polymers under Electromagnetic Radiation," *Polymers* 16 (2024): 689, https://doi.org/10.3390/polym16050689.

37. N. S. Allen, M. Edge, and S. Hussain, "Perspectives on Yellowing in the Degradation of Polymer Materials: Inter-Relationship of Structure, Mechanisms and Modes of Stabilisation," *Polymer Degradation and Stability* 201 (2022): 109977, https://doi.org/10.1016/j.polymdegradstab.2022.109977.

38. S. Cheng, H. Liu, S. Li, J. Cai, S. Liao, and F. Zhao, "Excellent Hydrophobic, Superior Ozone and UV Resistant, and High Thermal Stable Films from Bio-Based Natural Rubber Latex via Fluorinating under Mild Conditions," *Journal of Applied Polymer Science* 140 (2023): e54309, https://doi.org/10.1002/app.54309.

39. S. Liang, M. Wang, W. Gao, H. Diao, and J. Luo, "Recyclable, UV-Blocking, and Radiative Cooling Multifunctional Composite Membranes," *ACS Omega* 7 (2022): 25244, https://doi.org/10.1021/acsomega.2c02162.

40. S. Liu, C. Sui, M. Harbinson, et al., "A Scalable Microstructure Photonic Coating Fabricated by Roll-to-Roll "Defects" for Daytime Subambient Passive Radiative Cooling," *Nano Letters* 23 (2023): 7767, https://doi.org/10.1021/acs.nanolett.3c00111.

41. X. Li, L. Pattelli, Z. Ding, et al., "A Novel BST@TPU Membrane with Superior UV Durability for Highly Efficient Daytime Radiative Cooling," *Advanced Functional Materials* 34 (2024): 2315315, https://doi.org/10.1002/adfm.202315315.

42. C. Liu, Y. Wu, D. Li, T. Ma, A. K. Hussein, and Y. Zhou, "Investigation of Thermal and Optical Performance of a Phase Change Material-Filled Double-Glazing Unit," *Journal of Building Physics* 42 (2018): 99, https://doi.org/10.1177/1744259117708734.

43. C. Liu, J. Bian, G. Zhang, D. Li, and X. Liu, "Influence of Optical Parameters on Thermal and Optical Performance of Multi-Layer Glazed Roof Filled with PCM," *Applied Thermal Engineering* 134 (2018): 615, https://doi.org/10.1016/j.applthermaleng.2018.01.117.

44. L.-P. Wang, P.-D. Han, Z.-X. Zhang, C.-L. Zhang, and B.-S. Xu, "Effects of Thickness on the Structural, Electronic, and Optical Properties of MgF_2 Thin Films: The First-Principles Study," *Computational Materials Science* 77 (2013): 281, https://doi.org/10.1016/j.commatsci.2013.04.031.

45. A. Aili, Z. Y. Wei, Y. Z. Chen, D. L. Zhao, R. G. Yang, and X. B. Yin, "Selection of Polymers with Functional Groups for Daytime Radiative Cooling," *Materials Today Physics* 10 (2019): 100127, https://doi.org/10.1016/j.mtphys.2019.100127.

46. NIST Chemistry WebBook, https://webbook.nist.gov/chemistry/.

47. X. Song, Y. Gao, and P. Zhang, "Optical Properties of the Polymeric Radiative Cooler with Embedded Nano/ Micro-Particles," *Renewable and Sustainable Energy Reviews* 200 (2024): 114556, https://doi.org/10.1016/j.rser.2024.114556.

48. C. -C. Chang, C. -M. Huang, Y. -H. Chang, and C. Kuo, "Enhancement of Light Scattering and Photoluminescence in Electrospun Polymer Nanofibers," *Optics Express* 18 (2010): A174, https://doi.org/10.1364/OE.18.00A174.

49. J. C. Jonsson, L. Karlsson, P. Nostell, G. A. Niklasson, and G. B. Smith, "Angle-Dependent Light Scattering in Materials with Controlled Diffuse Solar Optical Properties," *Solar Energy Materials and Solar Cells* 84 (2004): 427, https://doi.org/10.1016/j.solmat.2004.02.048.

50. J. -L. Kou, Z. Jurado, Z. Chen, S. Fan, and A. J. Minnich, "Daytime Radiative Cooling Using Near-Black Infrared Emitters," *ACS Photonics* 4 (2017): 626, https://doi.org/10.1021/acsphotonics.6b00991.

26884062, 2026, 5, Downloaded from https://onlinelibrary.wiley.com/doi/10.1002/sstr.70462 by Lorenzo Pattelli - Universita Di Firenze Sistema , Wiley Online Library on [17/05/2026]. See the Terms and Conditions (https://onlinelibrary.wiley.com/terms-and-conditions) on Wiley Online Library for rules of use; OA articles are governed by the applicable Creative Commons License

51. Y. Tan, B. Liu, S. Shen, and Z. Yu, "Enhancing Radiative Energy Transfer through Thermal Extraction,"*Nanophotonics* 5 (2016): 22, https://doi.org/10.1515/nanoph-2016-0008.

52. G. Viswanadam and G. G. Chase, "Contact Angles of Drops on Curved Superhydrophobic Surfaces," *Journal of Colloid and Interface Science* 367 (2012): 472, https://doi.org/10.1016/j.jcis.2011.11.004.

53. N. M. D. Brown, J. A. Hewitt, and B. J. Meenan, "X-RAY Photoelectron-Spectroscopy and Infrared Studies of X-Ray-Induced Beam Damage of Cellulose, Ethyl Cellulose, and Ethyl-Hydroxyethyl Cellulose," *Surface and Interface Analysis* 18 (1992): 199, https://doi.org/10.1002/sia.740180305.

54. A. Kamaruddin, T. Wilujeng, and M. S. Mahendra, "*Radiative Cooling for Storage of Vegetables in the Tropics*," (2000): 702.

55. N. Saha, R. Benlikaya, P. Slobodian, and P. Saha, "Breathable and Polyol Based Hydrogel Food Packaging," *Journal of Biobased Materials and Bioenergy* 9 (2015): 136, https://doi.org/10.1166/jbmb.2015.1515.

56. S. Hahn and D. Hennecke, "What Can We Learn from Biodegradation of Natural Polymers for Regulation?," *Environmental Sciences Europe* 35 (2023): 50.

Supporting Information

Additional supporting information can be found online in the Supporting Information section.

26884062, 2026, 5, Downloaded from https://onlinelibrary.wiley.com/doi/10.1002/sstr.70462 by Lorenzo Pattelli - Universita Di Firenze Sistema , Wiley Online Library on [17/05/2026]. See the Terms and Conditions (https://onlinelibrary.wiley.com/terms-and-conditions) on Wiley Online Library for rules of use; OA articles are governed by the applicable Creative Commons License